ORIGINAL ARTICLE

lajss.org© Latin American Journal of Solids and Structures

www.lajss.org

Numerical and theoretical analysis of geosynthetic encased stone column composite foundation under cyclic loading

Junli Gao[a*], Xuelei Xie[a], Jiajun Wang[a], Lu Liu[a], Wenjie Zhang[a]

[a] School of Mechanics and Engineering Science, Shanghai University, Shanghai 200072, China.E-mails: susan_jl@staff.shu.edu.cn, xiexuelei@shu.edu.cn, shuwjj@shu.edu.com, 1144710472@shu.edu.cn, zhwjlyl@163.com

* Corresponding author

https://doi.org/10.1590/1679-78256979

Abstract

In this paper, a model of the composite foundation reinforced with geosynthetic encased stone columns was established using the discrete element method, and the characteristics of its action under cyclic loading were studied. The influence of the length and radius of the pile on the settlement of the composite foundation is analyzed. The deformation characteristics of the pile and the stress ratio of pile-soil are studied under different pile lengths and radius. Then, based on this, the analysis of the lateral deformation characteristics of the piles under cyclic loading, the calculation model of the geosynthetic encased pile composite foundation is established. The settlement calculation formula of the composite foundation is solved according to the deformation coordination relationship between the pile and soil, the equilibrium condition, and the boundary condition. The results show that the theoretical value is in good agreement with the simulation value, which verifies the rationality of the theoretical calculation formula.

Keywords

Cyclic loading; Numerical simulation; Encased stone column; Settlement caculation; reinforced soil

Graphical Abstract

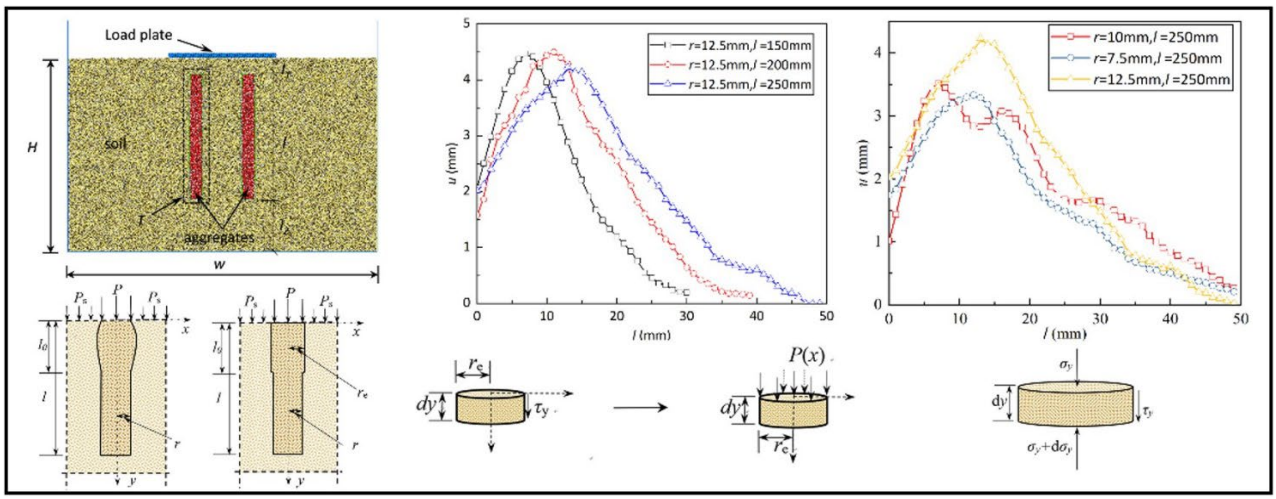

Received January 24, 2022. In revised form February 10, 2022. Accepted February 10, 2022.Available online February 10, 2022
https://doi.org/10.1590/1679-78256979

1 INTRODUCTION

The expressway and railway in China are developed rapidly in recent twenty years. However, soft soil foundations will inevitably be encountered in expressway and railway construction because of the limitation of geographical conditions such as low shear strength, a large void ratio, high water content, strong compressibility, and rheological properties. These characteristics are easy to induce uneven settlement and lateral sliding failure of the foundation under the repeated action of fixed load and traffic load on the pavement, resulting in the failure of the soft foundation to achieve the expected goal. Therefore, the soft soil foundation must be strengthened in order to meet the bearing capacity and deformation requirements.

The geosynthetic encased pile, based on the traditional stone column but wrapped with geosynthetics, is the most widely used method in soft soil foundation treatment. It not only retains the advantages of the traditional stone column, which can effectively improve the bearing capacity of the foundation, accelerate the drainage and consolidation of the soil, has little impact on the environment, convenient construction, low cost, etc., but also overcomes the disadvantage that the pile body is prone to bulge failure. The performance of geosynthetic encasement on the capacity and settlement behaviour of soft soils has been studied in both laboratory and field tests (Ayadat and Hanna, 2005; Murugesan and Rajagopal, 2010; Ali et al., 2012; Hosseinpour et al., 2015). Meanwhile, multiple researchers have carried out fruitful research on the deformation and settlement characteristics of stone column composite foundations (Zhang and Zhao,2015; Castro and Sagaseta,2011; Pulko et al.,2011). Afshar (Afshar and Ghazavi, 2014) and Lo (Lo et al.,2010) studied the effects of geotechnical materials on the bearing capacity of stone columns and their failure modes. Bongiorno (Bongiorno et al, 2006) and Malarvizhi (Malarvizhi and Ilamparuthi,2004) studied the effects of the reinforcement's stiffness and aspect ratio on the bearing capacity of geosynthetic encased piles and verified that reinforcement could effectively improve their stiffness and bearing capacity. Tan (Tan et al., 2018) found that geosynthetics had an obvious effect on the bearing capacity of the stone columns and the settlement of the composite foundation. Hosseinpour (Hosseinpour et al,2014) studied the influence of geosynthetics on the bearing capacity of stone columns and the settlement of the composite foundation by numerical simulation. Yoo (Yoo, 2015) explored the effective reinforcement depth of a geosynthetic encased pile by numerical simulation. Khabbazian (Khabbazian et al., 2015) studied the stress process of the wrapped material in a three-dimensional state by using three kinds of numerical analysis models and explored the relationship between the vertical and horizontal tensile stress of the geogrid. Kahyaoğlu and Vaníček (Kahyaoğlu and Vaníček, 2019) studied the three-dimensional finite element parameterization of the floating column on the soft soil foundation and discussed the influence of geogrid foundation reinforcement and geotextile wrapping on the column displacement characteristics. Borges and Marques (Borges and Marques, 2011) used a computer code based on the finite element method to analyze the time-dependent behaviour of a geosynthetic-reinforced, and jet grout column-supported embankment on soft soils, Niu (Niu et al., 2018) established a heavy instrumented high pile embankment model, and carried out model tests, measured the earth pressure, settlement, strain of geogrid and pile and excess pore water pressure under dynamic load. Tang (Tang et al.,2020) presented a small-scale model test to study the possible changes in stress distribution and deformation in the geosynthetic-reinforced pile foundations under increasing dynamic loads. In contrast, the influence of dynamic loads has received only modest attention. Most of the existing studies are focused on experiments and numerical simulation. In contrast, there are relatively few theoretical studies on encased stone columns, especially for the settlement calculation of encased stone columns under dynamic load.

This paper introduces the basic principle of encased stone column to reinforce the soft soil, and establishes the settlement calculation model of encased stone column composite foundation based on the integral expression of the displacement of the rigid circular support plate in the semi-infinite elastic solid and deformation coordination theory. The settlement of the encased stone columns with different pile lengths and pile radius under dynamic loads was calculated by using the formula. By establishing a discrete element numerical model, the influence of different pile lengths and pile radius on the bearing capacity and deformation of the foundation was further analyzed, and the results were compared with the formula calculation results. The results show that the formula used in this paper can accurately calculate the settlement of the encased stone column under different working conditions.

2 NUMERICAL SIMULATION OF COMPOSITE FOUNDATION

2.1 Establishment of particle flow model

In this study, the DEM model of encased stone column composite foundations was established by PFC2D since the discrete element method is suitable for analyzing the deformation and stress of bulk materials under periodic load. The composite foundation model is W = 600 mm in width and H = 330 mm in height. The thickness of the upper cushion is l_1 = 30 mm. The thickness of the underlying layer is l_2 = 80 mm. The width of the loading board is D = 290 mm. First, the 'ball' cell is used to generate the foundation soil according to a certain gradation. In order to improve the calculation efficiency, the soil particle radius is appropriately enlarged, and the number of particles is 22286. Since the foundation soil simulated in this paper is sand, the contact

mode between soil particles adopts a linear contact model. Then the soil particles at the position of the encased stone columns are deleted, and the wrapping material and aggregate particles are generated at the same position. The parallel bonding model is used between the particles of the wrapping material to transmit the tensile force and moment, which simulates a constraining effect of the wrapping material on the aggregate. The contact adopted between aggregate particles is also a linear contact model, but in order to reflect the mechanical occlusal effect between aggregates, the friction coefficient between particles is appropriately increased. Finally, a 'clump' cell is generated on the ground surface to simulate the loading plate. During the loading process, the settlement of the foundation is represented by recording the vertical displacement of the loading plate. The bulge at different depths of the pile body was calculated by recording the lateral displacement of the particles of the wrapping material. Fig.1 shows the composite foundation of geosynthetic encased piles. The dotted line T in Fig.1 is the analysis diagram of one single pile model, which is shown in Fig. 2 (a).

When the model is established, the vertical force is applied to the 'clump' for loading. The cyclic loading waveform applied in the simulation is a half sine wave, the 110 peak load is 1500 N, the frequency is 1 Hz, and the number of cycles is 1500.

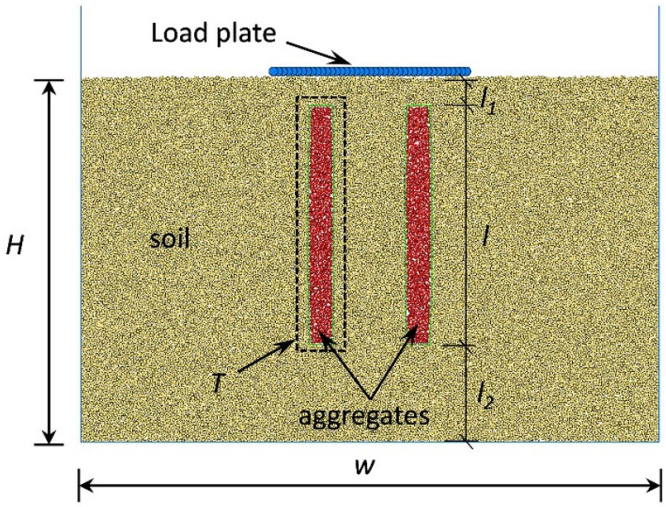

Figure 1 Composite foundation of reinforced stone column

2.2 Macro and micro parameters of simulated materials

In order to provide satisfactory DEM simulation results and refer to the existing experimental data (Wang et al.,2016), the linear modulus of the wrapping material of the stone column is set to 2e7 MPa, the linear stiffness ratio is 1.0 and the bond modulus is 1e12. The micro input parameters in the composite foundation are calibrated. The physical and mechanical properties of sand and aggregates are obtained by establishing the numerical model of biaxial test. The physical and mechanical properties of the simulated sand are as follows: the Poisson's ratio of the sand is μ_s = 0.3, the Young's modulus of the sand is E_s = 10 MPa. The physical and mechanical properties of the aggregates are as follows: the Poisson's ratio of the aggregates μ_a = 0.25, the elastic modulus of the aggregates E_a = 30 MPa, and the internal friction angle of the aggregates φ_a = 35°.

2.3 Simulation working conditions

In the simulation process, the settlement change of composite foundation is analyzed by changing the pile radius and pile length of the stone column in the composite foundation. The simulation condition in this paper is shown in Table 1.

Table 1 Working conditions of numerical simulation

number	*r*/mm	*l*/mm	remarks
A[1]	/	/	control group
B	7.5	250	/
C	10.0	250	/
D	12.5	250	/
E	12.5	150	/
F	12.5	200	/

A[1]: pure sand foundation

3 THEORETICAL ANALYSIS OF SETTLEMENT OF COMPOSITE FOUNDATION

The total settlement of the composite foundation with geosynthetic encased stone columns under cyclic loading consists of three parts: pile settlement w_1, settlement of upper cushion w_2, settlement of underlying layer w_3 (Appendix 1), which can be expressed as:

$$w = mw_1 + w_2 + w_3 \tag{1}$$

Where w is the total settlement of the composite foundation (mm), m is defined as the ratio of cyclic displacement which are presented in Appendix 1, which is related to the bearing capacity of a single pile under static load, the amplitude of cyclic loading and the properties of the soil around the pile (Guo et al., 2015). The settlement w_2 of the upper cushion is very small, and can be ignored in the calculation process. The calculation method of the settlement w_3 of the underlying layer is simple. Therefore, the key to the settlement of the composite foundation with the geosynthetic encased stone columns lies in the calculation of the pile settlement w_1.

3.1 Basic assumptions and calculation models

When calculating the settlement of the composite foundation with geosynthetic encased stone columns, due to the interaction of the pile and soil, the stress situation is complicated. Several simplifying assumptions are usually made to make the problem simpler with reference to major factor:

1. The stone columns and the surrounding soil are linear elastic materials.
2. The effect of the self-weight stress of the piles and soil on the compression deformation of the composite foundation is not considered.
3. Ignoring the influence of the pile group's effect on the mechanical properties of the element, the settlement and deformation of the composite foundation are approximately analysed by the "pile-soil element".
4. The settlement of the pile and the soil around the pile at the same depth is equal.

Brauns (Brauns,1978) considered that the stone column will produce bulging deformation under the vertical load as shown in Fig. 2. Therefore, the bulging failure length can be given by:

$$l_0 = 2r\,tan\left(45^\circ + \frac{\varphi_a}{2}\right) \tag{2}$$

Where l_0 is the depth of bulging failure along the pile direction (mm), r is the initial radius of the stone column (mm), and φ_a is the internal friction angle (°) of the pile material, which are presented in Appendix 1.

In this paper, the pile is divided into a bulging area and non-bulging area. Due to the bulging deformation of the upper half of the pile, it is difficult to determine the pile radius, which makes the calculation difficult. Therefore, an equivalent radius r_e is introduced into the calculation in this paper. r_e can be calculated from Eqs. (3)-(4):

$$S_1 = S_0 + \int_0^{l_0} y(x)\,dx \tag{3}$$

$$r_e = \frac{S_1}{S_0} r \tag{4}$$

Where: S_0 is the initial cross-sectional area of the stone column (mm^2), and S_1 is the cross-sectional area (mm^2) of the pile in the bulging area, see Appendix 1, S_0=2rl_0.

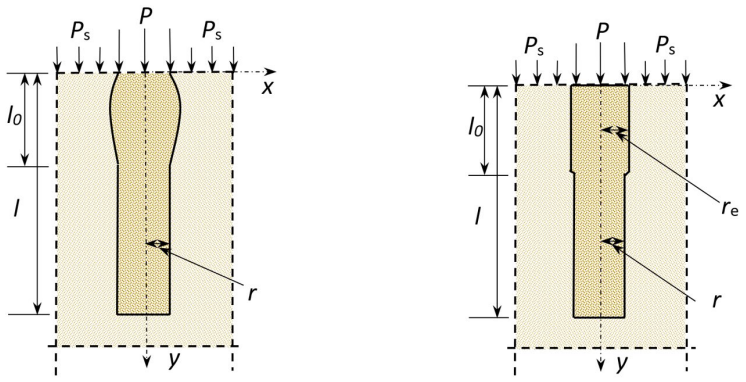

(a) The analysis diagram of a single pile model (b) Equivalent calculation model

Figure 2 Bulging deformation diagram of pile after loading

3.2 Settlement calculation

3.2.1 Settlement of any point in soil surrounding pile

Fig. 2 (b) presented calculation model of single pile after equivalent analysis of bulging area. Take the pile-soil interface for analysis, as shown in Fig. 3. The settlement of the soil around the pile consists of three parts: the settlement w_{PR} caused by the pile end counterforce; the settlement w_{uu} and w_{tt} caused by the skin friction of the pile, and the settlement w_{Ps} caused by the load on the upper part of the soil around the pile, which are described in Appendix 1.

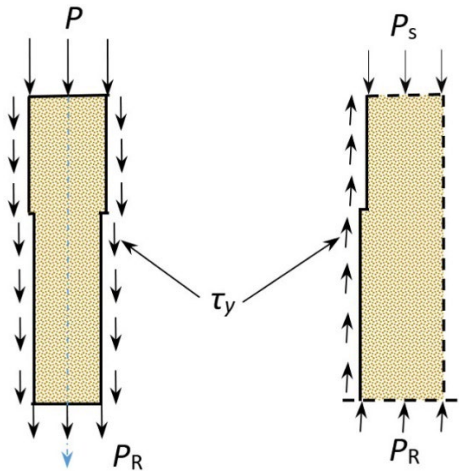

Figure 3 Analysis model of pile-soil interface

The composite foundation load is transferred to the soil at the pile end, P_R is the pile end counterforce (presented in Appendix 1), and the distribution of the pressure stress of the soil at the pile end under the pile end counterforce is as follows:

$$f = \frac{2P_R}{\pi r^2} \tag{5}$$

Where f is the compressive stress value of the lower edge of the circular bearing plate, P_R is the pile end counter force (N), see Appendix 1.

The settlement of soil under the pile end counterforce is w_{PR}, which is presented in Appendix 1. Through the integral expression of the displacement of the rigid circular support plate in the semi-infinite elastic body, the settlement expression of the soil under the pile end can be obtained:

$$w_y = \frac{(1+\mu_s)fr}{2E_s}\alpha_1 \tag{6}$$

Where μ_s is the Poisson's ratio of sand and E_s is the Young's modulus of sand, which are shown in Appendix 1. δ and α_1 are parameters demonstrated as:

$$\delta = 2(1-\mu_s) \tag{7}$$

$$\alpha_1 = 2(1-\mu_s)\left(\frac{\pi}{2} - arctan\frac{y}{r}\right) + \frac{yr}{y^2+r^2} \tag{8}$$

Substituting Eq. (5) into Eq. (6) gives:

$$w_{PR} = \frac{\beta_R(1-\mu_s^2)P_R}{E_s r} \tag{9}$$

Where β_R is the correction factor for settlement calculation (Appendix 1), which is determined by the physical and mechanical properties of the soil around the pile, the length and radius of the pile and other parameters. Generally, the value is 0.5 ~1.0 (Zhang et al., 2013), and it is 0.65 in this paper.

The settlement of the soil around the pile caused by the skin friction is w_{uu} and w_{tt}, respectively. Take a section of the bulging area of the stone column for analysis as shown in Fig. 4. In order to simplify the calculation, the pile skin friction is equivalent transformed.

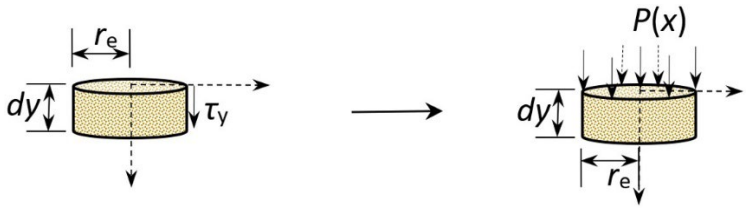

Figure 4 Equivalent transformation of pile skin friction

The conversion formula of pile skin friction is as follows:

$$\int_0^{2\pi} \frac{2(1-\mu_s^2)\tau_y}{2\pi E_s r_e} r_e dy d\theta = \frac{2P(x)r_e(1-\mu_s^2)}{E_s} \tag{10}$$

Where τ_y is the pile skin frictional resistance, which is presented in Appendix 1

$$P(x) = \frac{\tau_y}{r_e} dy \tag{11}$$

Then, the settlement of the soil surrounding the pile caused by the skin friction of the pile in the bulging area and the non-bulging area is as follows:

$$w_{uu} = \int_0^{l_0} \frac{\beta_R \tau_{uy}(1+\mu_s)}{2E_s} \alpha_2 dy \tag{12a}$$

$$w_{tt} = \int_{l_0}^{l} \frac{\beta_R \tau_{ty}(1+\mu_s)}{2E_s} \alpha_3 dy \tag{12b}$$

Where α_2 and α_3 are parameters demonstrated as:

$$\alpha_2 = \delta\left(\frac{\pi}{2} - arctan\frac{y}{r_e}\right) + \frac{yr_e}{y^2+{r_e}^2} \tag{13a}$$

$$\alpha_3 = \delta\left(\frac{\pi}{2} - arctan\frac{y-l_0}{r}\right) + \frac{(y-l_0)r}{(y-l_0)^2+r^2} \tag{13b}$$

The load of the soil around the pile of the composite foundation is P_s. The settlement of the soil under the load of the soil around the pile can be solved according to the formula of the displacement of the half space under the action of the concentrated load, and the settlement of the soil can be solved integrally within the long strip range:

$$w_{Ps} = \frac{4\beta_R P_s D(1+\mu_s)}{\pi E_s}[\eta + \chi] \tag{14}$$

Where P_s is the upper load of soil around the pile, D is half the width of the loading plate (Appendix 1). η and χ are parameters demonstrated as:

$$\eta = \delta\left(\sqrt{1+\frac{y^2}{D^2}} - \frac{y}{D}\right) \tag{15}$$

$$\chi = \frac{y}{D}\left[1 - \frac{y}{D}\left(1+\frac{y^2}{D^2}\right)^{-0.5}\right] \tag{16}$$

According to the above Eqs. (9) - (14), the settlement of the soil around the pile under various loads can be obtained, and the settlement of each part can be accumulated to any point of the soil around the pile.

$$w_{11} = w_{PR} + w_{uu} + w_{tt} + w_{Ps} \tag{17}$$

3.2.2 Settlement of any point on the pile

The settlement of any point on the pile consists of three parts: the settlement w_{PRa} of the soil at the pile end; the settlement w_{uua} and w_{tta} of the soil at the pile end due to the skin friction of the pile (presented in Appendix 1), and the compression deformation of the pile itself under the load of the pile top. It can be seen from Eq. (6) that the settlement of the soil mass at the pile end under the reaction of the pile end is as follows:

$$w_{PRa} = \frac{\zeta_R P_R(1-\mu_s^2)}{rE_s} \tag{18}$$

Where ζ_R is the correction factor for settlement calculation (Appendix 1), which is determined by the physical and mechanical properties of the soil around the pile, the length and radius of the pile and other parameters. Generally, the value is 0.5 ~ 1.0 (Zhang et al., 2013), and it is 0.65 in this paper.

The settlement of the pile bottom caused by the skin friction in the bulging area and the non-bulging area is as follows:

$$w_{uua} = \int_0^{l_0} \frac{\xi_R \tau_{uy}(1+\mu_s)}{2E_s}\alpha_4 dy \tag{19a}$$

$$w_{tta} = \int_{l_0}^{l} \frac{\xi_R \tau_{ty}(1+\mu_s)}{2E_s}\alpha_5 dy \tag{19b}$$

Where α_4 and α_5 is a parameter demonstrated as:

$$\alpha_4 = \delta\left(\frac{\pi}{2} - arctan\frac{l_0-y}{r_e}\right) + \frac{(l_0-y)r_e}{(l_0-y)^2+{r_e}^2} \tag{20a}$$

$$\alpha_5 = \delta\left(\frac{\pi}{2} - arctan\frac{l-y}{r}\right) + \frac{(l-y)r}{(l-y)^2+r^2} \tag{20b}$$

According to the internal stress distribution of the stone column, the compression deformation of the stone column in the bulging area and non-bulging area are as follows:

$$w_{ua} = \int_0^{l_0} \frac{1}{E_a}\left[\sigma_{uy} - 2\mu_a \frac{\tau_{uy}}{tan\varphi_a}\right] dy \tag{21a}$$

$$w_{ta} = \int_{l_0}^{l} \frac{1}{E_a}\left[\sigma_{ty} - 2\mu_a \frac{\tau_{ty}}{tan\varphi_a}\right] dy \tag{21b}$$

Where E_a is the Young's modulus of stone column, σ_{uy} and σ_{ty} are the axial stress of pile body in the bulging and non-bulging area respectively, and μ_a is the Poisson's ratio of the pile body (Appendix 1).

According to the above Eqs. (18) -(21b), the settlement of the pile under various loads can be obtained, and finally the final settlement of each part is settled and accumulated:

$$w_{12} = w_{PRa} + w_{uua} + w_{tta} + w_{ua} + w_{ta} \tag{22}$$

3.3 Pile soil stress balance

Take a certain segment of stone column for analysis, as shown in Fig. 5.

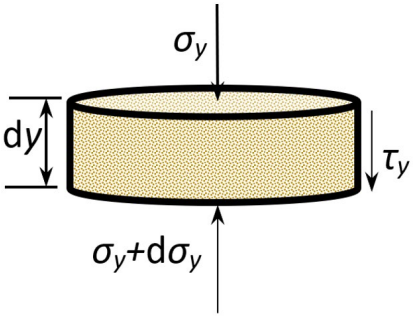

Figure 5 Stress diagram

According to the force balance of the element segment, the balance equation can be obtained:

$$\left(\sigma_y + d\sigma_y\right)\pi r^2 + 2\pi r\tau_y dy = \sigma_y \pi r^2 \tag{23}$$

Eliminating the term of Eq. (23) gives:

$$rd\sigma_y + 2\tau_y dy = 0 \tag{24}$$

At the top of the stone column, $y = 0$, the axial force σ_y of the pile is:

$$\sigma_y = \frac{P}{\pi r^2} \tag{25}$$

Where P is the top load of the stone column (presented in Appendix 1).
At the bottom end of the stone column, $y = l$, the axial force σ_y of the pile is:

$$\sigma_y = \frac{P_R}{\pi {r_e}^2} \tag{26}$$

4 Settlement calculation formula solution

The stress parameters (σ_y, τ_y, P_R, see Appendix 1) can be determined by the force balance and deformation coordination relationship between the piles and the soil. The settlement of the composite foundation is calculated from the soil and pile directions respectively. According to the assumption of equal strain, that is, that the settlement of the pile and the soil at the same depth is equal before the pile and soil break away under the load.

$$w_{11} = w_{12} \tag{27}$$

Combining Eq. (24) and Eq. (27) rearranged: Eq. 6, substituting them into Eqs. (25)-(26) gives:

$$\sigma_y = \frac{P}{\pi {r_e}^2}\left[\rho + \kappa_1 \frac{\beta_R}{\xi_R} + \frac{4\beta_R P_s(1+\mu_s)}{\pi r_e(1-\mu_s^2)} n_1\right] \tag{28}$$

Where ρ, κ_1 and n_1 are parameters demonstrated as:

$$\rho = exp\left(\frac{B}{A^2} ln\left(\frac{Ay+B}{B}\right) - \frac{y}{A}\right) \tag{29}$$

$$\kappa_1 = exp\left(\frac{B}{A^2} ln\left(\frac{A(l_0-y+r_e)+B}{B}\right) - D\right) \tag{30}$$

$$D = \frac{l_0-y-r_e}{A} \tag{31}$$

$$n_1 = \delta(D + y - \sqrt{y^2+D^2}) + y\left(\frac{y}{\sqrt{y^2+D^2}} - 1\right) \tag{32}$$

$$\tau_y = \frac{P}{2\pi r_e}\left[\rho v + \kappa_1 \frac{\beta_R}{\xi_R}\psi_1\right] + \frac{2\beta_R P_s(1+\mu_s)}{\pi(1-\mu_s^2)}\zeta \tag{33}$$

Where v, ψ_1 and ζ are parameters demonstrated as:

$$v = \frac{y}{Ay+B} \tag{34}$$

$$\psi_1 = \frac{l_0-y+r_e}{A(l_0-y+r_e)+B} \tag{35}$$

$$\zeta = (1-2\mu_s)\left(\left(\frac{y}{\sqrt{y^2+D^2}} - 1\right) - \frac{yD^2}{(y^2+D^2)^{1.5}}\right) \tag{36}$$

$$P_R = f\frac{\beta_R}{\xi_R}\theta_1 + \frac{4\beta_R P_s r_e(1+\mu_s)}{(1-\mu_s^2)} n_2 \tag{38}$$

Where ϑ_1 and n_2 are parameters demonstrated as:

$$\theta_1 = exp\left(\frac{B}{A^2} ln\left(\frac{Ar_e+B}{B}\right) - \frac{r_e}{A}\right) \tag{39}$$

$$n_2 = \delta(D + l_0 - \sqrt{{l_0}^2+D^2}) + l_0\left(\frac{l_0}{\sqrt{{l_0}^2+D^2}} - 1\right) \tag{40}$$

In the non-bulging area of the pile:
The upper load F_1 of non-bulging area (listed in Appendix 1) is:

$$P_1 = F - \int_0^{l_0} 2\pi r_e \tau_y dy \tag{41}$$

Where τ_y is the skin friction of the pile in the bulging area (see Appendix 1).

$$\sigma_y = \frac{P_1}{\pi r^2}\left[\rho + \frac{\beta_R}{\xi_R}\kappa_2 + \frac{4\beta_R P_s(1+\mu_s)}{\pi r(1-\mu_s^2)} n_1\right] \tag{42}$$

Where κ_2 is a parameter demonstrated as:

$$\kappa_2 = exp\left(\frac{B}{A^2} ln\frac{A(l-y+r)+B}{B} - \frac{l-y-r}{A}\right) \tag{43}$$

$$\tau_y = \frac{P_1}{2\pi r}\left[\rho v + \frac{\beta_R}{\xi_R}\kappa_2\psi_2 + \frac{2\beta_R P_s(1+\mu_s)}{\pi(1-\mu_s^2)}\zeta\right] \tag{44}$$

Where ψ_2 is a parameter demonstrated as:

$$\psi_2 = \frac{l-y+r}{A(l-y+r)+B} \tag{45}$$

$$P_R = P_1\frac{\beta_R}{\xi_R}\theta_2 + \frac{4\beta_R P_s r(1+\mu_s)}{1-\mu_s^2}n_3 \tag{46}$$

Where ϑ_2 is a parameter demonstrated as:

$$\theta_2 = exp\left(\frac{B}{A^2}ln\left(\frac{Ar+B}{B}\right) - \frac{r}{A}\right) \tag{47}$$

$$A = \frac{\mu_a r_e}{tan\varphi_a}, \quad B = \frac{3\pi E_a {r_e}^2(1-\mu_s)}{16E_s} \tag{48}$$

Substituting the above formulas into Eq. (17) and Eq. (19), the total settlement of the stone column can be calculated. In the calculation model of stone column composite foundation in this paper, because the interaction between geogrid and soil particles between piles can effectively reduce the settlement of soil between piles in composite foundation, considering the above reasons, a correction coefficient is introduced to correct the settlement of soil on the pile side.

Then the settlement of composite foundation is:

$$w_1 = \lambda w_{11} = \lambda w_{12} \tag{49}$$

$$w_2 = \frac{Pl_2}{E_s} \tag{50}$$

Where: λ is the correction coefficient, which is presented in Appendix 1, and λ is taken as 0.75 through the numerical simulation results. w_2 is the amount of compression of the sand cushion. l_2 is the thickness of the sand cushion. w_3 is the amount of settlement of the underlying layer soil, the amount of which can be calculated directly according to the code for design of building foundations, and then the amount of settlement of the foundation can be calculated.

5 Results and analysis

5.1 Calculation of equivalent radius of bulging area

Fig. 6 shows the change of lateral displacement along the pile length during the tests.

It can be known from Fig. 6 that after the loading is completed, the pile body will undergo a certain bulging deformation along the direction of the pile body. The deformation effect is different under different pile lengths and radius. When the pile length is constant, as the radius of the pile increases, the range of bulging will gradually increase, which is consistent with the research by Brauns (Brauns, 1978). When the radius of the pile is constant, the range of bulging of the pile is basically the same. As the length of the pile increases, the location where the maximum bulging deformation occurs will gradually deepen.

The values of radius r_e of the bulging area under different pile radius and pile lengths can be obtained by curve fitting with Eqs. (3)-(4).

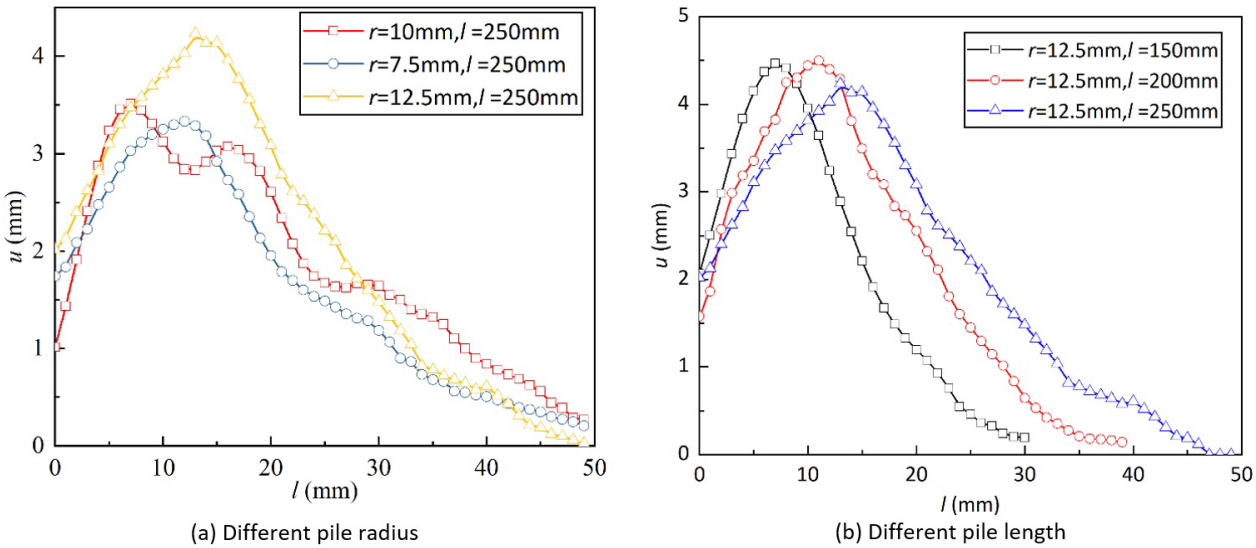

(a) Different pile radius (b) Different pile length

Figure 6 The radial deformation along the depth curve of the pile

5.2 Stress concentration ratio

In the initial loading stage of cyclic loading, the stress concentration ratio of geosynthetic encased stone column composite foundation increases rapidly with the increase of the number of loadings and then gradually tends to a certain limit value. The stress concentration ratio under different pile radius and lengths is obtained by numerical simulation, as shown in Table 2.

Table 2 illustrates the stress concentration ratio under various working conditions. It shows that the stress concentration ratio increases with the increase of the pile radius and length. Therefore, the soil mass tends to be more stable, as confirmed in the load shared by the piles in the composite foundation increases gradually.

Table 2 Pile-soil stress ratio under various working conditions

Number	*r*/mm	*l*/mm	Pile-soil stress ratio
A	/	/	control group
B	7.5	250	3.91
C	10.0	250	7.07
D	12.5	250	9.2
E	12.5	150	4.91
F	12.5	200	6.26

When the applied load is known, the upper load of the pile and the upper load of the soil between piles can be solved by the following formula.

$$n = \frac{P}{P_s} \tag{51}$$

Where: n is the stress concentration ratio; P is the upper load of the pile; P_s is the upper load of the soil surrounding the pile, which are described in Appendix 1.

5.3 Result verification and analysis

5.3.1 Influence of pile radius on settlement of composite foundation

Fig. 7 shows the vibration time settlement curve of dynamic load under different working conditions. It shows that the settlement of the geosynthetic encased pile composite foundation with different pile radius has little difference at the initial stage of loading. With the increase of the loading times, the difference in settlement of the geosynthetic encased pile composite foundation with different pile radius increases gradually. At the beginning of loading, the settlement of the model increases rapidly. However, the settlement of the model decreases gradually with the increase of the loading times, and the settlement curve becomes gentle. At the end of loading, the settlement of the model

decreases with the increase of the pile radius of the geosynthetic encased stone column, which shows that geosynthetic encased pile plays an obvious role in reducing the settlement of the foundation.

5.3.2 Influence of pile length on settlement of composite foundation

Fig. 7 (b) shows the dynamic load vibration time settlement curve of the composite foundation with geosynthetic encased stone columns with a pile radius of 12.5 mm is taken for analysis, and the pure sand foundation model is also taken as the control group. The difference in settlement of the geosynthetic encased pile composite foundation model with pile lengths of 200 mm and 250 mm in the early stage of loading is not significant. With the increase of the loading times, this difference increases gradually, and settlement of the model increases rapidly in the early stage of loading, while the trend of the settlement curve of the model gradually slows down with the increase of the loading times.

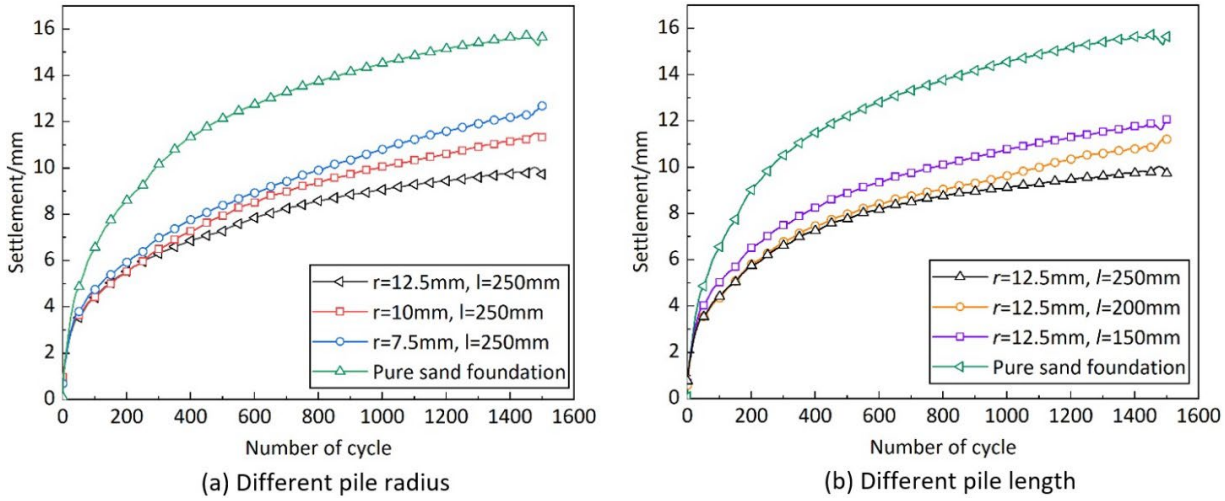

Figure 7 The vibration time settlement curve of dynamic load under different working conditions.

5.3.3 Comparison of simulated and theoretical results

The pile settlement value can be obtained by substituting the equivalent radius of the bulging area under different pile radius and pile lengths, the upper load of the pile body and the upper load of the soil between piles into Eq. (1), as shown in Table 3.

It can be seen from Table 3 that the calculated value of the settlement under cyclic loading is basically consistent with the numerical simulation data, and the maximum error between them is not more than 16%, which shows that it is feasible to divide the pile into bulging and non-bulging areas for analysis when calculating this settlement.

In order to study the influence of the pile length and pile radius on the settlement of the composite foundation, the results of numerical simulation and theoretical calculation under different pile radius and lengths are compared Fig.8 shows the relationship between the settlement of composite foundation and the pile length and radius.

Table 3 Comparison of theoretical and numerical results under different working conditions

r/mm	r_e/mm	l/mm	w_a^1 /mm	w/mm	per/%
7.5	11.20	250	11.62	12.62	8.6
10	12.96	250	10.48	10.82	3.3
12.5	13.91	150	11.54	9.70	-16.0
12.5	15.04	200	10.46	10.89	4.1
12.5	14.84	250	9.29	10.25	10.3

Note: w_a^1 refers to the settlement value of numerical simulation

According to Fig. 8, when the pile length is fixed, the total settlement of the geosynthetic encased stone column composite foundation decreases with the increase of the pile radius, indicating that the settlement of the composite foundation can be significantly reduced by increasing the replacement rate of the composite foundation. When the pile radius is fixed, the total settlement of the geosynthetic encased pile composite foundation changes little with the increase of the stone column length. The results show that when the pile radius is fixed, the effect of the pile on the composite foundation increases less with the increase in the pile length.

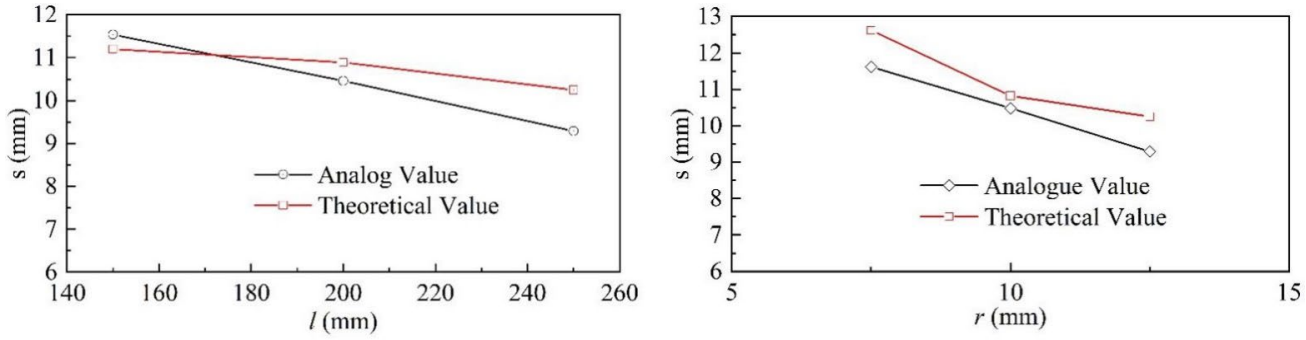

(a) Different pile length (b) Different pile radius

Figure 8 Settlement curve of composite foundation with pile length and pile radius

6 CONCLUSIONS

In this paper, particle flow software is used to simulate the geosynthetic encased pile composite foundation under cyclic loading and to analyse the stress and deformation and, on this basis, calculation of the foundation settlement under cyclic loading is theoretically deduced. Through numerical simulation and theoretical calculation, the following conclusions are reached.

- The calculated results in this paper are consistent with the simulation results, and the maximum error is no more than 16%. The results show that it is feasible to divide the stone column into expansion zone and non-expansion zone in the settlement calculation and analysis of the model. The calculation method in this paper can accurately reflect the settlement of encased stone column composite foundation.
- The numerical simulation and theoretical calculation results show that, compared with pure sand foundation, the encased stone column can effectively reduce the settlement of the foundation by about 25%-40%. Increasing pile radius and pile length of the encased stone column can improve the replacement rate of composite foundation and increase the foundation stiffness, so as to reduce the settlement of foundation under cyclic loading.
- The simulation results show that under cyclic loading, the bulging deformation occurs in the upper part of the encased stone column, resulting in foundation settlement. When the pile length is fixed, the bulging zone will gradually increase with the increase of the pile radius. When the pile radius remains unchanged, the maximum bulging position will gradually deepen with the increase of pile length.

Acknowledgments:

The research described in this paper was financially supported by the National Natural Science Foundation of China (Grant numbers No. 41772300)

Author's Contribuitions: Conceptualization, J Gao; Methodology, W Zhang; Investigation, X Xie, J Wang, L Liu; Writing - original draft, *X* Xie, J Wang, L Liu; Writing - review & editing, J Gao and X Xie; Funding acquisition, W Zhang; Resources, J Gao and W Zhang; Supervision, J Gao.

Editor: Rogério José Marczak

References

Ayadat, T., Hanna, A.M. (2005). Encapsulated stone columns as a soil improvement technique for collapsible soil. Ground Improvement. 9(4): 137–147.

Ali, K., Shahu, J.T., Sharma, K.G. (2012). Modeltests on geosynthetic-reinforced stone columns: A comparative study. Geosynthetics International. 19(4): 292–305.

Afshar, J. N., & Ghazavi, M. (2014). Experimental studies on bearing capacity of geosynthetic reinforced stone columns. Arabian Journal for Science and Engineering. 39(3): 1559-1571.

Brauns, J. (1978). The initial load of stone column in the clay foundation. The construction technology. 55(8): 263-271.

Bongiorno, D., Cantarelli, E., DI PRISCO, C. G., Galli, A. (2006). Geo-reinforced sand columns: Small scale experimental tests and theoretical modelling. In Proceedings of the 8th international conference on geosynthetics. pp. 1685-1688.

Borges, J.L., Marques, D.O. (2011). Geosynthetic-reinforced and jet grout column-supported embankments on soft soils: Numerical analysis and parametric study. Computers and Geotechnics. 38(7): 883-896.

Castro, J., Sagaseta, C. (2011). Deformation and consolidation around encased stone columns. Geotextiles and Geomembranes. 29(3): 268-276.

Guo, P.F., Wang, X., Yang, l.C., & Luo, H.W. (2015). Model test study on settlement characteristics of single pile in Loess under long-term vertical cyclic load. Journal of geotechnical engineering. 37 (3): 551-558. (in Chinese).

Hosseinpour, I., Riccio, M., Almeida, M. S. (2014). Numerical evaluation of a granular column reinforced by geosynthetics using encasement and laminated disks. Geotextiles and Geomembranes. 42(4): 363-373.

Hosseinpour, I., Almeida, M.S.S., Riccio, M. (2015). Full-scale load test and finite-element analysis of soft ground improved by geotextile-encased granu-lar columns. Geosynthetics International. 22(6): 428-438.

Khabbazian, M., Kaliakin, V. N., Meehan, C. L. (2015). Column supported embankments with geosynthetic encased columns: validity of the unit cell concept. Geotechnical and Geological Engineering. 33(3): 425-442.

Kahyaoğlu, M. R., Vaníček, M. (2019). A NUMERICAL STUDY OF REINFORCED EMBANKMENT-SUPPORTED BY ENCASED FLOATING COLUMNS. Acta Geotechnica Slovenica. 2.

Lo, S. R., Zhang, R., Mak, J. (2010). Geosynthetic-encased stone columns in soft clay: a numerical study. Geotextiles and Geomembranes. 28(3): 292-302.

Malarvizhi, S. N., Ilamparuthi, K. (2004). Load versus settlement of clay bed stabilized with stone and reinforced stone columns. In 3rd Asian Regional Conference on Geosynthetics. pp. 322-329.

Murugesan, S., Rajagopal, K. (2010). Studies on the behavior of single and group geosynthetic encased stone columns. Journal of Geotechnical and Geoenvironmental Engineering. 136(1): 129-139.

Niu, T., Liu, H., Ding, X., Zheng, C. (2018). Model tests on XCC-piled embankment under dynamic train load of high-speed railways. Earthquake Engineering and Engineering Vibration. 17(3): 581-594.

Pulko, B., Majes, B., Logar, J. (2011). Geosynthetic-encased stone columns: analytical calculation model. Geotextiles and Geomembranes. 29(1): 29-39.

Tan, X., Zhao, M., Chen, W. (2018), Numerical Simulation of a Single Stone Column in Soft Clay Using the Discrete-Element Method. International Journal of Geomechanics. 18(12): 1-12.

Tang, Y., Xiao, S., & Yang, Q. (2020). The behaviour of geosynthetic-reinforced pile foundation under long-term dynamic loads: model tests. Acta Geotechnica. 1-21.

Wang, Z., Jacobs, F., & Ziegler, M. (2016). Experimental and DEM investigation of geogrid–soil interaction under pullout loads. Geotextiles and Geomembranes. 44(3): 230-246.

Yoo, C. (2015). Settlement behavior of embankment on geosynthetic-encased stone column installed soft ground–a numerical investigation. Geotextiles and Geomembranes. 43(6): 484-492.

Zhang, M.J., Luo Q., Zhan X.Q., et al. (2013). Settlement analysis of settlement calculation of CFG pile composite foundation of high-speed railway. Rock and Soil Mechanics. (02): 219-225 + 245. (in Chinese)

Zhang, L., & Zhao, M. (2015). Deformation analysis of geotextile-encased stone columns. International Journal of Geomechanics. 15(3): 1-10.

Appendix 1

D width of the loading board (mm)
E_a Young's modulus of the gravel pile (MPa)
E_s Young's modulus of the sand (MPa)
F_1 the upper load of non-bulging area (N)
f compressive stress value of the lower edge of the circular bearing plate (MPa)
H height of composite foundation model (mm)
l length of pile (mm)
l_0 depth of bulging failure (mm)
l_1 thickness of the upper cushion (mm)
l_2 thickness of the underlying layer (mm)
m ratio of cyclic displacement (-)
n stress concentration ratio
P the top load of the gravel pile (N)
P_R pile end counterforce (N)
P_s load of the soil surrounding the pile (N)
r initial radius of pile (mm)
r_e equivalent radius (mm)
S_0 initial cross-sectional area of the gravel pile (mm^2)
S_1 cross-sectional area of pile in the bulging area (mm^2)
u lateral displacement of pile (mm)
W width of composite foundation model (mm)
w total settlement of the composite foundation (mm)
w_1 pile settlement (mm)
w_2 settlement of upper cushion (mm)
w_3 settlement of underlying layer (mm)
w_a^1 settlement value of numerical simulation
w_{PR} settlement caused by the pile end counterforce (mm)
w_{PRa} settlement of the soil at the pile end (mm)
w_{Ps} settlement caused by the load P_s(mm)
w_{ta} compression deformation in the non-bulging area (mm)
w_{tt} settlement caused by the skin friction of pile (mm)
w_{tta} settlement of the pile bottom caused by τ_{ty} (mm)
w_{ua} compression deformation in the bulging area (mm)
w_{uu} settlement caused by the skin friction of pile (mm)
w_{uua} settlement of the pile bottom caused by τ_{uy} (mm)
β_R correction factor for settlement calculation (-)
ζ_R correction factor for settlement calculation (-)
μ_a Poisson's ratio of the gravel pile (-)
μ_s Poisson's ratio of the sand (-)
σ_{ty} the axial stress of pile body in non-bulging area
σ_{uy} the axial stress of pile body in the bulging area
τ_y pile skin frictional resistance (-)
φ_a internal friction angle of the gravel pile (°)